Digest Journal of Nanomaterials and Biostructures Vol. 20, No. 4, October-December 2025, p. 1621-1638

Comparative investigation on specific heat capacity of Cd and Ta-doped BV for pyroelectric energy harvesting

K. Swethaa [a], M. Rajeswari [a,*], L. Balakrishnan [b]
[a] *Department of Physics, Government College of Engineering, Bodi -625582, Tamil Nadu, India.*
[b] *Department of Physics, Government College of Technology, Coimbatore -641013, Tamil Nadu, India.*

Ferroelectric bismuth vanadate (BV) has been investigated for its specific heat capacity (C_p), which is one of the most prime factors for determining pyroelectric performance through pyroelectric figures of merit (PyFOM). BV was separately doped with cadmium (Cd) and tantalum (Ta) d-block transition metals to perform a comparative analysis of the impact created by both dopants on BV. Various concentration of both metals was doped for the effective study (say 1atomic percent (%), 3%, 5% and 7% of dopants). The undoped and doped samples were synthesized through the hydrothermal method. X-ray diffraction (XRD) was performed on all samples, which revealed that BV had a monoclinic structure, and the crystallite size calculated by the aid of the Cauchy-Lorentzian formula increased on doping Cd. Whereas Ta doping reduced the crystallite size. The cubical morphology of BV was confirmed through field emission scanning electron microscopy (FESEM). The constitution of elements was analysed through energy dispersive X-ray analysis (EDAX), which substantiated the appearance of required elements in the samples. The ultraviolet diffuse reflectance spectrometer (UV-DRS) authenticated the narrowed indirect bandgap with a 2.4 eV range, broad absorption range (200–550 nm), and reflectance of undoped and doped BV samples. X-ray photoelectron spectroscopy (XPS) revealed the chemical states and binding energy of all elements exist within the samples. The thermogravimetric analysis (TGA) associated with differential scanning calorimetry (DSC) was performed to obtain data on loss of weight and flow of heat in the samples. The C_p calculated from the TGA-DSC data for Cd-doped BV was found to increase, and that of Ta-doped BV was found to decrease.

(Received September 22, 2025 Accepted December 27, 2025)

Keywords: Bismuth vanadate, Cadmium, Tantalum, Pyroelectric figures of merit, hydrothermal, Specific heat capacity

1. Introduction

Pyroelectricity is the measure of electric charges generated by a temperature fluctuation developed within the material on exposing to heat or cool sources. The temperature fluctuation causes a spontaneous polarization thereby produces a pyroelectric voltage and the material from which the pyroelectric current or voltage is yieldable on exposing to different sources of temperature is called the pyroelectric material. All ferroelectric materials have pyroelectric property and belong to the subclass of dielectric materials. In this work, the ferroelectric bismuth vanadate (BV) was investigated for its specific heat capacity (Cp) which is regarded as a crucial factor to influence the pyroelectric enhancement in the material. The C_p is inversely proportional to the pyroelectric figures of merit (PyFOM) say current responsivity (F_I), voltage responsivity (F_V) and detectivity (F_D) which determines the material's performance towards pyroelectric charge generation. Owing to the inverse proportionality of PyFOM to C_p, the material with very low C_p can produce better PyFOM values which in turn increases the pyroelectric efficiency [1-3]. Furthermore, the polymorphic material BV was doped with the d-block transition metals cadmium (Cd) and tantalum (Ta) for reducing the C_p of pure BV which can favour for improvising the pyroelectric behaviour. The dopants were doped with different concentrations say 1 atomic percent (%), 3%, 5% and 7% in pure BV to study their effects in low-level and high-level doping. BV was effectively examined by the scientific community for its antimicrobial, photo-catalytic, supercapacitor, photoelectrochemical applications and not yet accounted for pyroelectric energy harvesting application [4-6]. The samples were characterized through X-ray diffraction (XRD), field emission scanning electron microscope

* Corresponding author: drmrajeswari30@gmail.com
https://doi.org/10.15251/DJNB.2025.204.1621

(FESEM), energy dispersive X-ray analysis (EDAX), ultra-violet diffuse reflectance spectrometer (UV-DRS), X-ray photoelectron spectrometer (XPS) and thermogravimetric analysis (TGA) with differential scanning calorimeter (DSC) for determining the material's crystal structure, crystallite size, lattice parameters, morphology, elemental composition, absorbance, reflectance, bandgap, binding energy and C_p. The undoped and doped BV were synthesized by the hydrothermal method, which is regarded as a facile route for the synthesis of powdered samples to obtain better results [7,8].

2. Materials and methods

The utilized precursors are bismuth nitrate pentahydrate (Bi $(NO_3)_3$.5H2O) and ammonium metavanadate (NH_4VO_3) and the precipitating agents are nitric acid (HNO_3) and sodium hydroxide (NaOH). Cadmium nitrate hexahydrate (Cd $(NO_3)_2$.6H2O) and tantalum oxide (Ta_2O_5) are used as dopants.

2.1. Pure BV preparation

The experiment is initiated by dissolving 2 ml of HNO_3 in 60 ml of deionized (DI) water contained within a beaker and stirred stirring gently with the aid of a magnetic stirrer. 0.5 mmol of Bi $(NO_3)_3$.5H2O is added to this solution and taken as solution A.

$$Bi(NO_3)_3 + HNO_3 \longrightarrow Bi(NO_3)_3 \text{ dissolves} \qquad \text{(Solution A)}$$

0.5 mmol of NH_4VO_3 was dissolved in another beaker containing 60 ml of DI water and mixed well for 30 min on a stirrer. 0.5 mmol of NaOH pellets were readily solubilized in 40 ml of DI water and poured into NH_4VO_3 solution. This solution was stirred well. In doing so, the solution turns to a transparent pale-yellow colour and is named as solution B. Now, solution B is poured into solution A which yields a proper yellow precipitated solution.

$$NH_4VO_3 + 3NaOH \longrightarrow Na_3VO_4 + NH_3 + 2H_2O \qquad \text{(Solution B)}$$

When solution B is added to solution A,

$$Bi(NO_3)_3 + Na_3VO_4 \longrightarrow BiVO_4 + 3NaNO_3 \qquad \text{(Solution A + B)}$$

The yellow colour of the solution confirms the formation of BV and is transferred to a Teflon container. The teflon container is then sealed in a stainless steel autoclave and maintained at 150 °C in a hot air oven for 24 h. Once the samples are cooled to room temperature, they are washed, dried at 80 °C, ground by mortar and pestle and placed in a muffle furnace at 400 °C for 2 h to obtain better results (Fig. 1) [7-9].

2.2. Cd and Ta-doped BV preparation

The Cd and Ta were doped separately in pure BV and were prepared with various doping concentrations to compare and analyse the difference in their properties. 1%, 3 %, 5 % and 7% of Cd $(NO_3)_3.6H_2O$ and Ta_2O_5 was added to the solution B before adding NaOH. Same sequence of experimental procedure is followed after adding Cd $(NO_3)_2.6H_2O$ and Ta_2O_5 separately to solution B. This results in the formation of 1%, 3%, 5%, 7% Cd and Ta-doped BV nano particles.

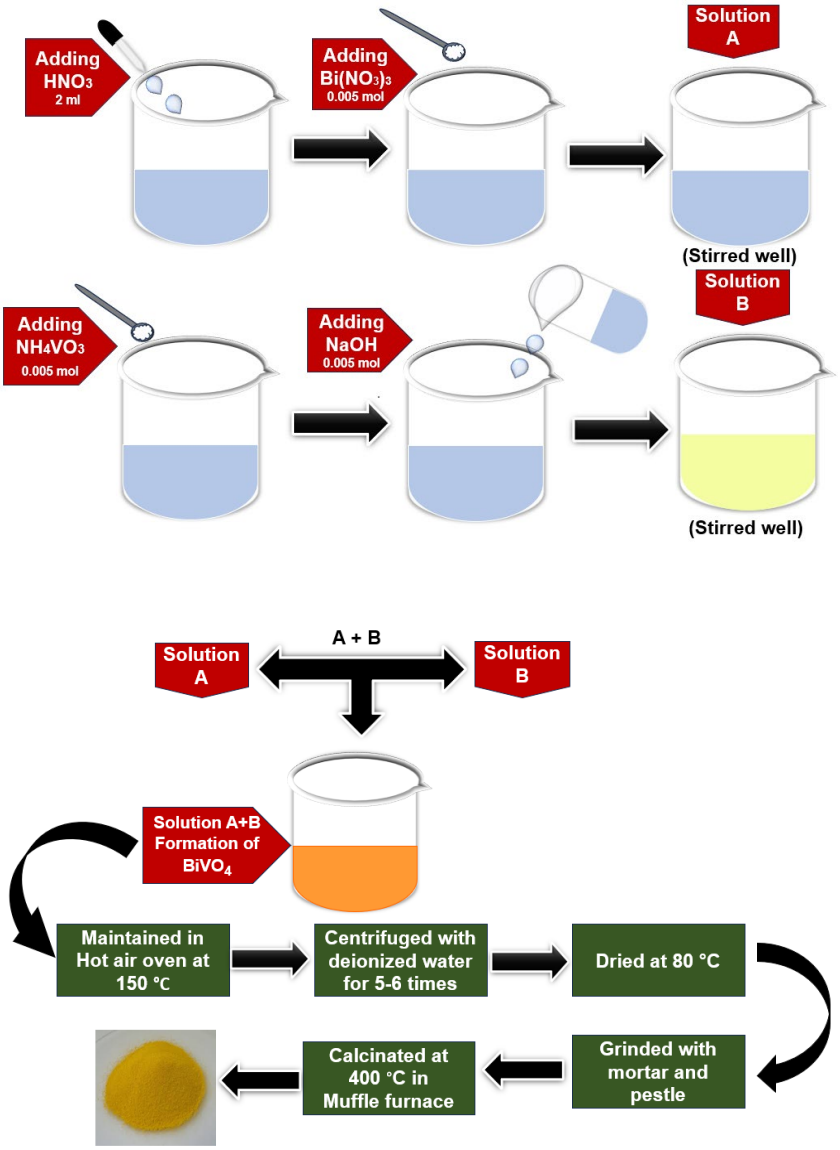

Fig. 1. Schematic representation for hydrothermal synthesis of BV nano particles.

3. Results and discussion

3.1. X-ray diffraction analysis

The XRD pattern in Fig. 2(a) and 2(b) shows the monoclinic scheelite structure (JCPDS card no. 14-0688) of pure, Cd and Ta-doped BV. Both Cd and Ta-doped BV show intensity variation when compared to pure BV as Cd and Ta atoms distort the BV lattice. The Cd^{2+} ions occupy the unoccupied Bi^{3+} sites and the Ta^{5+} ions take up the V^{5+} sites on the atomic lattice. All Cd-doped BV samples experience a lattice expansion assured by the left shift in the peak, which is noted in Fig. 2(c). The Cd ions with 0.97 Å ionic radius occupying the sites of Bi3+ ions having 1.03 Å ionic radius do not account for any extra peaks revealing that they are well anchored in the BV lattice. Whereas, the 5% and 7% Ta-doped BV convey the presence of Ta_2O_5 (0.64 Å ionic radius) peaks at 23° and 36° owing to the higher concentration doping of Ta_2O_5. The atomic scattering factor differs for 5% and 7% Ta-doped BV when compared to 1% and 3% Ta-doped BV attributed to the existence of Ta_2O_5 on the BV surface [10]. All the Ta-doped samples (except 5%) also suffer lattice expansion which is observed in the Fig. 2(d). Thus, Ta atoms not only shift the peaks by anchoring into the BV lattice but also functionalize the surface of monoclinic BV when doped in excess amounts. The size and strain of crystals in all samples were estimated through the Cauchy-Lorentzian formula,

$$\beta f \cos\theta = K\lambda/D + 4\varepsilon\sin\theta$$

were K-shape factor (K = 0.94), λ-wavelength of X-ray used, D-crystallite size, βf -full width half maximum and θ-Bragg's angle. Furthermore, the lattice constants were calculated manually using the interfacial angle β value obtained from JCPDS card (β = 90.38). The formula for calculating lattice constants of a monoclinic structure is,

$$\frac{1}{d^2} = \frac{1}{sin^2\beta}\left[\frac{h^2}{a^2} + \frac{k^2 sin^2\beta}{b^2} + \frac{l^2}{c^2} - \frac{2hlcos\beta}{ac}\right]$$

where d- interplanar spacing, h, k, l – Miller indices, a, b, c – lattice constants and β-interfacial angle [11]. Figs. 3 and 4 shows the Williamson-Hall plot of pure BV, Cd-doped BV and Ta-doped BV. The crystallite size of Cd-doped BV sample having low-intense XRD peaks found to be increased relative to pure BV and that of Ta-doped BV sample with high-intense peaks decreases. However, all samples have a perfect crystalline nature as they exhibit sharp peaks. Almost all samples exhibited a similarity in manually calculated a, b, and c values relative to the JCPDS card and validated to have an intact monoclinic structure [7].

Table 1. Calculated crystal size (D), strain (ε) and lattice constants (a, b, c) values of pure and doped BV.

Samples	Crystallite size 'D' nm	Strain 'ε'		Lattice constants(Å)	
			a (Å)	b (Å)	c (Å)
Pure BV	78.78	0.00176	5.149	11.582	5.047
1% Cd	81.56	0.00138	5.172	11.652	5.072
3% Cd	95.62	0.00156	5.166	11.628	5.064
5% Cd	89.45	0.00142	5.188	11.689	5.084
7% Cd	122.72	0.00156	5.192	11.688	5.088
1% Ta	47	0.00111	5.177	11.659	5.078
3% Ta	47.64	0.00261	5.160	11.580	5.063
5% Ta	51.16	0.00101	5.149	11.585	5.050
7% Ta	65.71	0.00121	5.166	11.628	5.065
JCPDS card no.14-0688			5.195	11.701	5.092

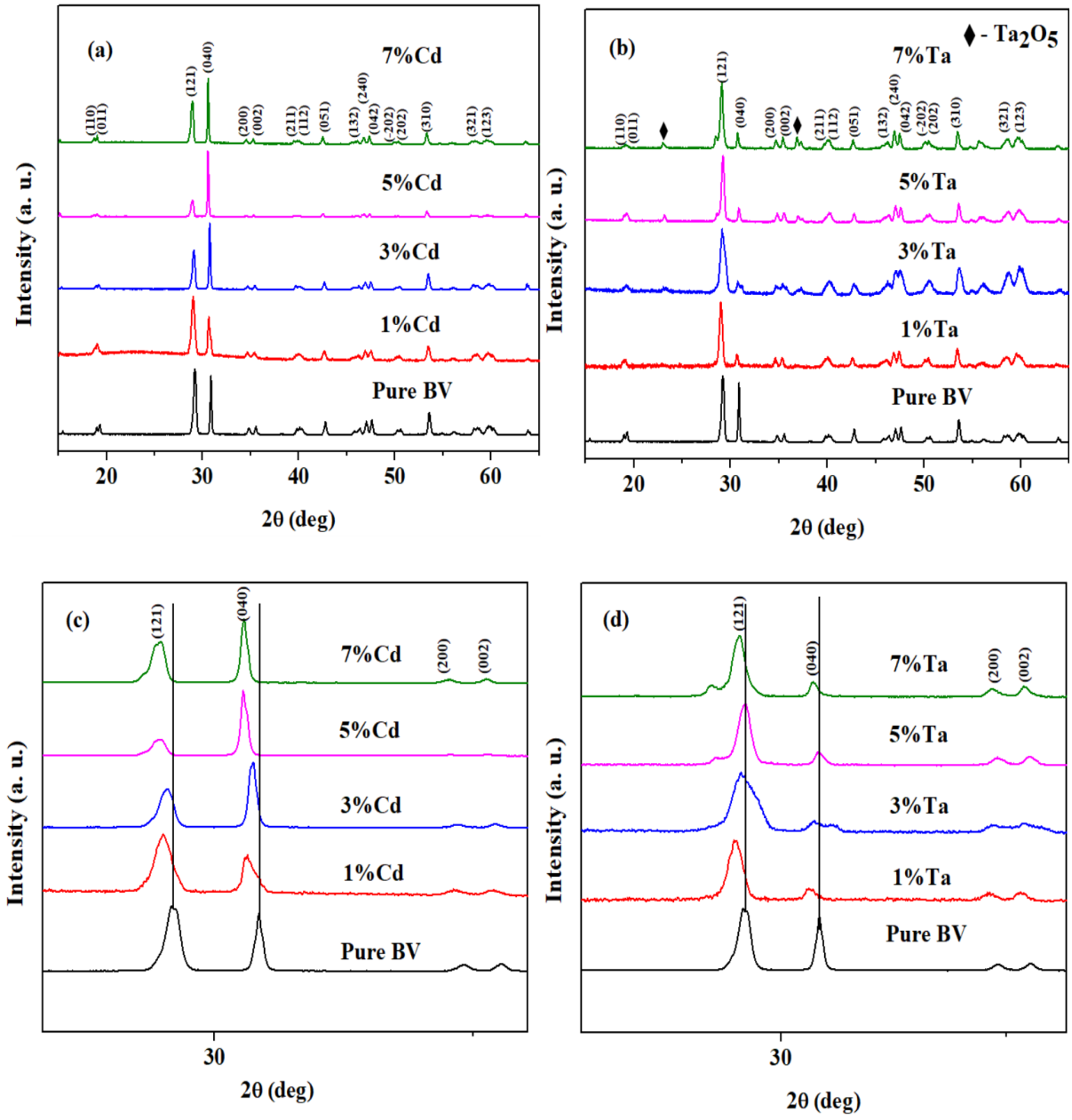

Fig. 2. XRD spectra of (a) Cd-doped BV and (b) Ta-doped BV. Lattice expansion in (c) Cd-doped BV and (d) Ta-doped BV.

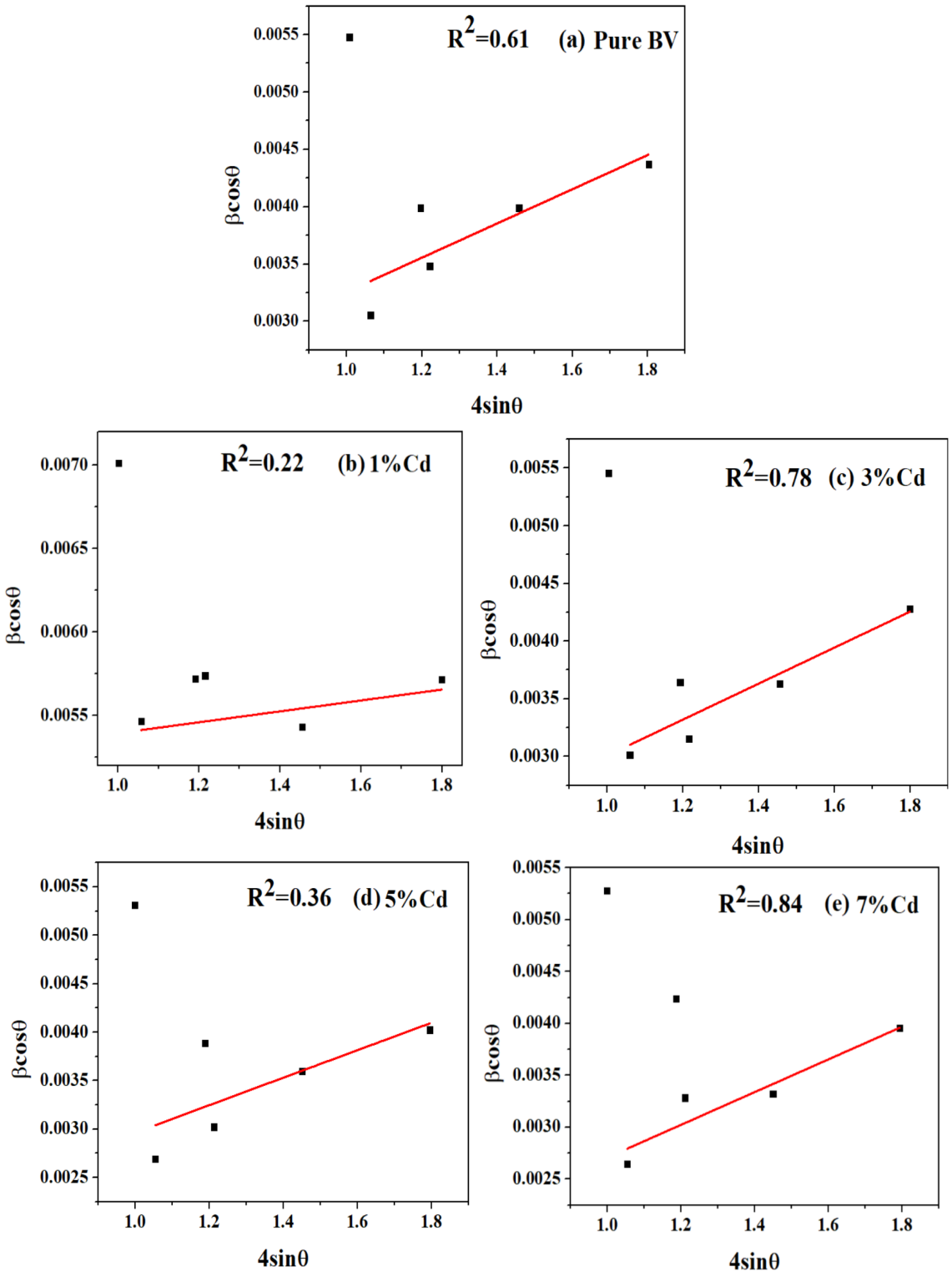

Fig. 3. W. H. plot of pure BV and Cd-doped BV.

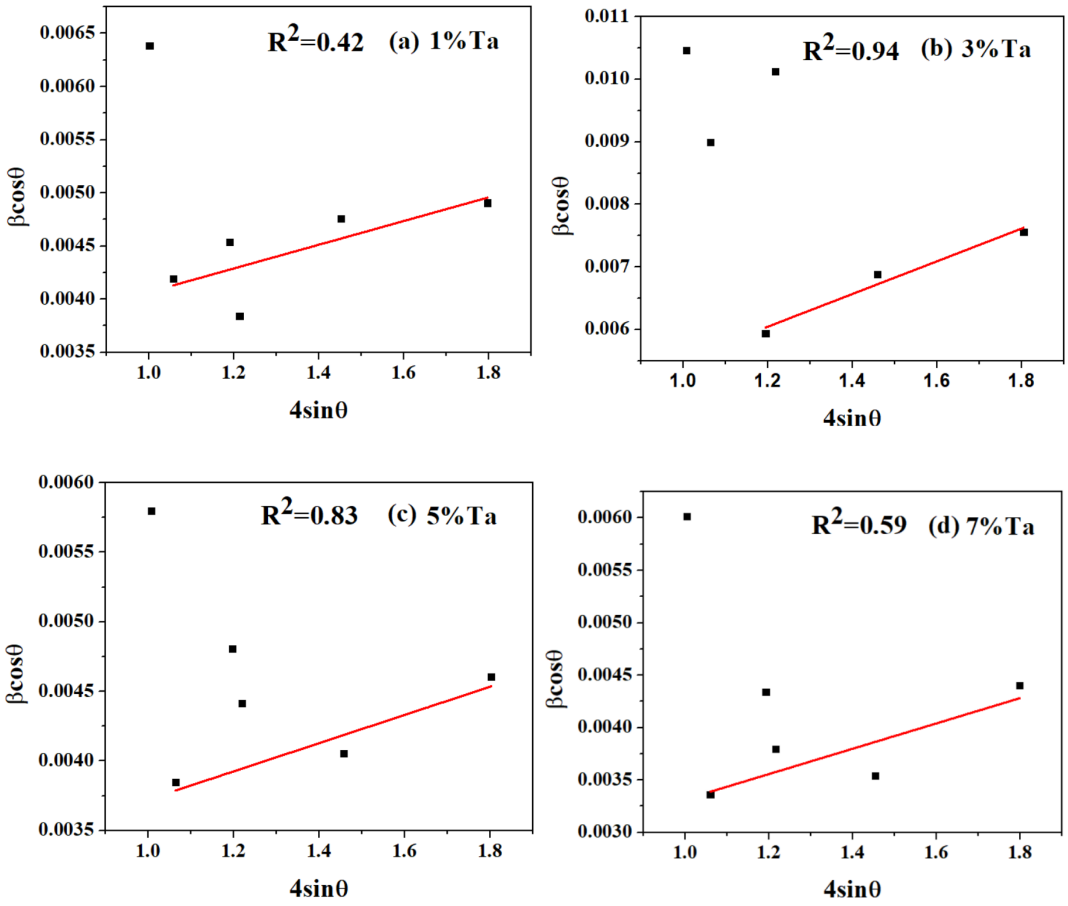

Fig. 4. W. H. plot of Ta-doped BV.

3.2. Field emission scanning electron microscopy and energy dispersive X-ray analysis

FESEM and EDAX technique is employed to analyse the surface morphology and the elemental ratio of the nano structures under examination. Pure BV, 7% Cd and Ta-doped BV was analysed through FESEM. They are identified to have a cubical morphology when recorded in the scale of 2 μm [12, 13]. As both 7% Cd and Ta-doped sample possess cubical morphology similar to pure BV it can be said that both dopants do not produce any significant variation on the morphology of pure BV and they remain to be micro cubes. The BV micro cubes possess highly active sites and larger surface area compared to other BV morphologies like nano spheres, nano rods etc., The exposure of these micro cubes to any kind of heat or cool source can provide better energy harvesting results owing to the large surface area, as the material's surface area is directly related to the quantity of energy generated. Fig. 5(a), 5(b) and 5(c) presents the morphology of pure BV, 7% Cd and Ta-doped BV. The EDAX data provided the composition and the ratio of constituents present within the samples. The Fig. 6(a) confirms the existence of bismuth (Bi), vanadium (V) and oxygen (O). Fig. 6(b) and 6(c) additionally confirms the presence of the dopants Cd and Ta.

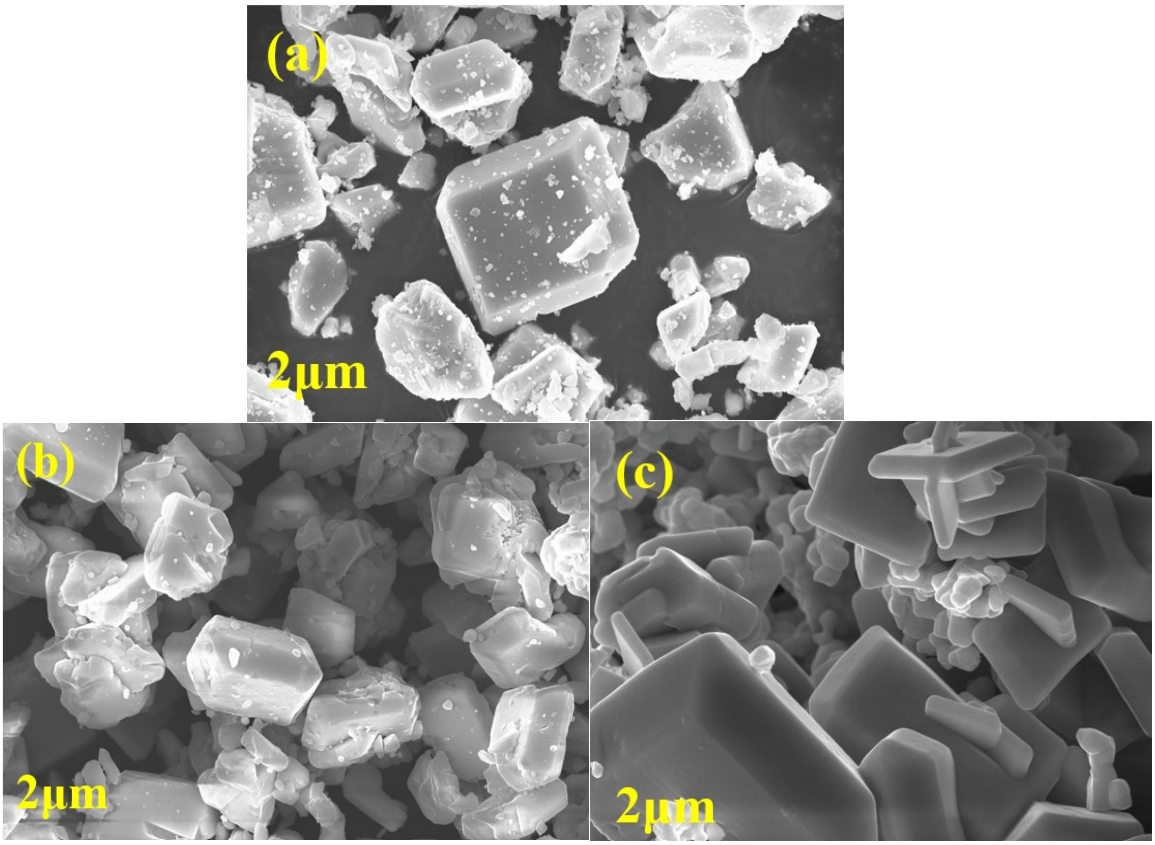

Fig. 5. FESEM images of (a) pure BV, (b) 7% Cd-doped BV and (c) 7% Ta-doped BV.

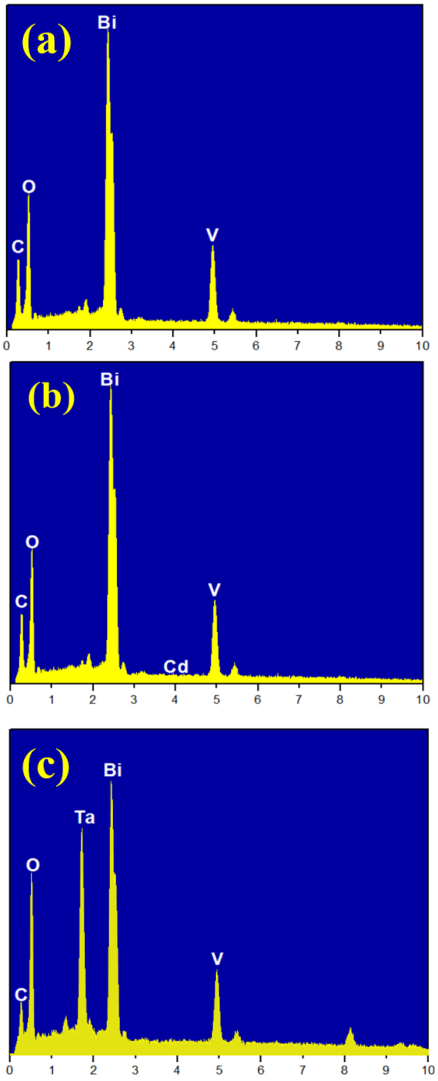

Elements	Weight %	Atomic %
CK	7.25	28.25
OK	13.13	38.43
BiM	57.34	12.85
VK	22.27	20.47

Elements	Weight %	Atomic %
CK	3.03	20.05
OK	20.22	48.87
BiM	61.72	15.84
VK	14.88	15.17
CdL	0.15	0.07

Elements	Weight %	Atomic %
CK	5.52	24.04
OK	12.72	41.57
BiM	44.27	11.08
VK	16.91	17.36
TaM	20.58	5.95

Fig. 6. EDAX images of (a) pure BV, (b) 7% Cd-doped BV and (c) 7% Ta-doped BV.

3.3. Ultraviolet- visible diffuse reflectance spectrometric analysis

The UV-DRS provides us the absorption and reflectance data which further help us to calculate the bandgap of the material. All samples show broad absorption and the absorption edge starts at 350 nm for pure BV and Cd-doped BV. While the absorption edge of Ta-doped BV suffers a red shift. The variation in the intensity of the absorption peaks is noted (Fig. 7(a) and 7(b)) due to the Cd and Ta doping with different concentrations. The reflectance spectra (Fig. 7(c) and 7(d)) allow us to determine the UV-scattering efficiency of the samples. The 1% and 3% Cd-doped BV and 3%, 5% and 7% Ta-doped BV offered a high UV reflection compared to other samples that can possibly hinder the pyroelectric detection capability which is least bothered, as the pyroelectric performance of a material mainly depends on the PyFOM. Attributed to the misalignment of valence and conduction bands the humps are noted in the absorption spectra which reveal the phonon-assisted charge transition from valence band to the intermediate level and then to the conduction band. The electrons, once after reaching the intermediate levels by absorbing photon energy are assisted by the phonons to reach the conduction band via indirect bandgap transition. In the case of BV, the bismuth 6s orbitals are overlapped on oxygen 2p orbitals to create the valence band while the vanadium 3d orbitals create the conduction band. The energy gap in all the samples was estimated by the Kubelka-Munk relation from the extrapolated linear portions (Fig. 8(a) and 8(b)). The Kubelka-Munk relation is,

$$F(R) = \frac{(1-R)^2}{2R} = \frac{K}{S}$$

F(R) is the Kubelka-Munk function, R is the reflectance of the material, K is the molar absorption coefficient and S is the scattering coefficient. The band gap of all samples lied around 2.4 eV which confirms the monoclinic nature of BV [11,14].

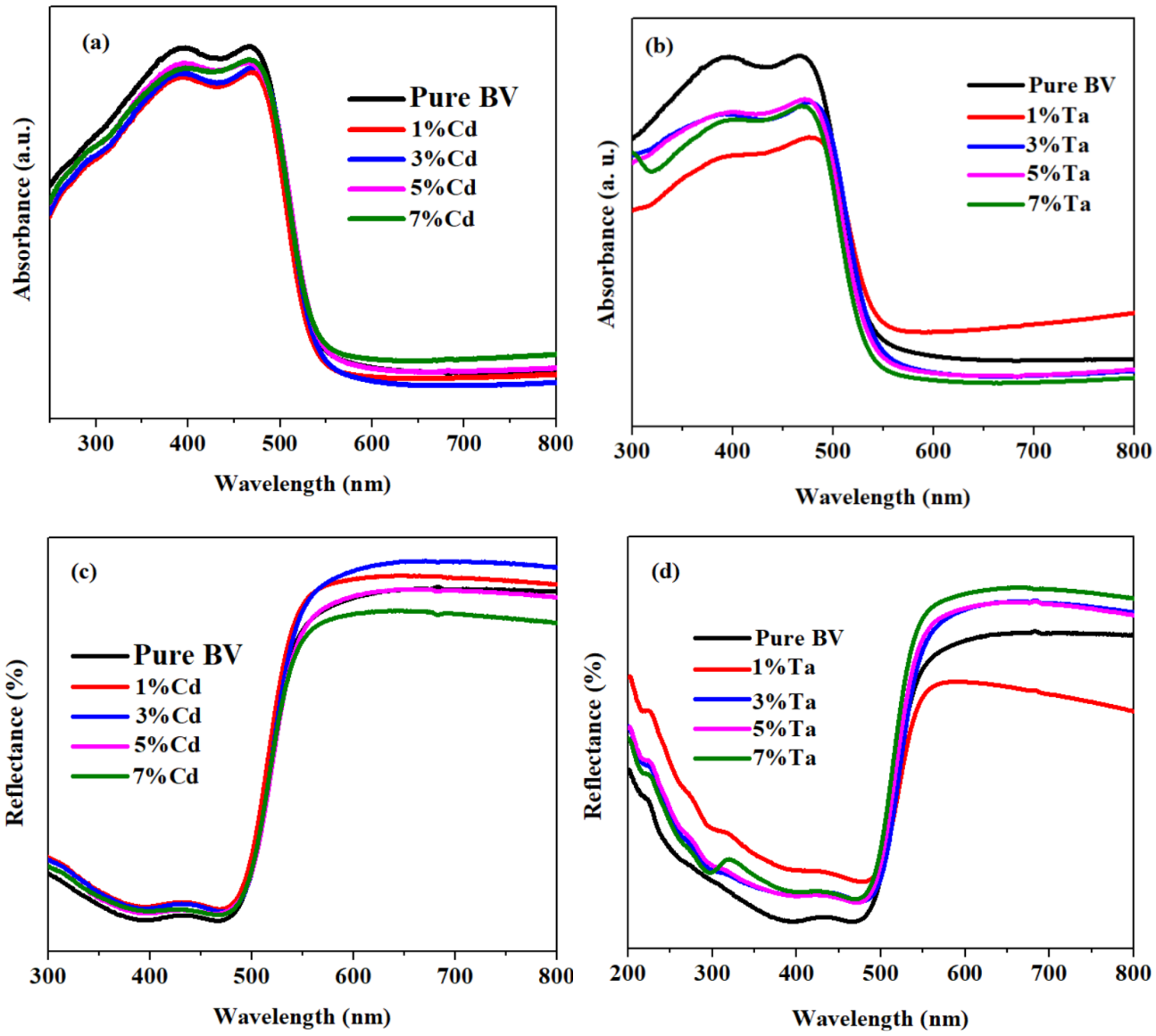

Fig. 7. UV absorbance spectra of (a) Cd-doped BV and (b) Ta-doped BV. UV reflectance spectra of (c) Cd-doped BV and (d) Ta-doped BV.

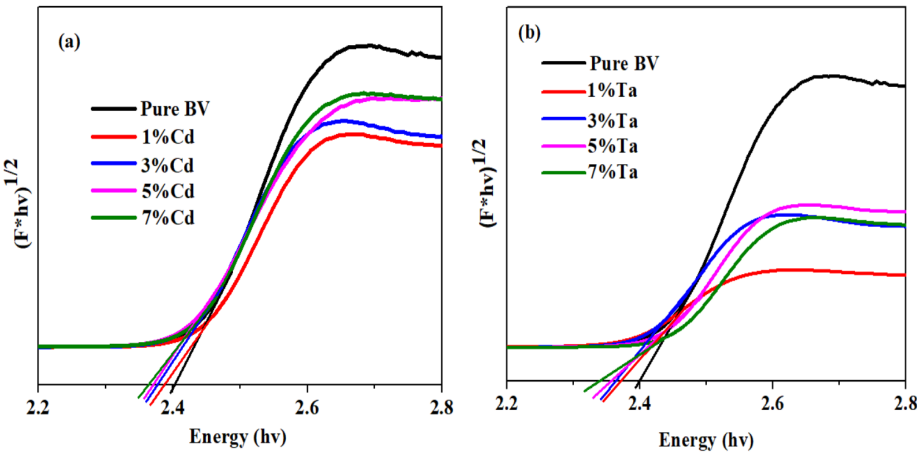

Fig. 8. Kubelka-Munk plots of (a) Cd-doped BV and (b) Ta-doped BV.

3.4. X-ray photoelectron spectrometric analysis

XPS was operated to determine the existing chemical states, binding energy and composition of elements of pure BV, 7% Cd and Ta-doped BV. Fig. 9(a) displays the survey spectrum of pure BV which confirms the presence of Bi 4f, Bi 4d, Bi 5d, Bi 4p, V 2p and O 1s chemical states in pure BV. Fig. 9(b) details the split of Bi 4f orbital into Bi $4f_{5/2}$ and Bi $4f_{7/2}$ orbital states with binding energies 158.6 eV and 163.9 eV. Fig. 9(c) specifies the binding energies of V 2p peaks at 516.3 eV (V $2p_{3/2}$) and 523.7 eV (V $2p_{1/2}$). Fig. 9(d) expound the chemical state of Oxygen (O 1s) which exists with a binding energy of 529.4 eV attributed to the lattice oxygen and other peak at 531.5 eV indicates the oxygen absorbed by Bi and V to become more stable as O is highly electronegative element. Fig. 10(a) articulates the survey spectrum of 7% Cd-doped BV and confirms the presence of Cd. All the elements showed an increase in binding energy (Fig. 10(b), (c) and (d)) due to Cd doping which confirms the highest stable nature of 7% Cd-doped BV relative to pure BV. The core level spectrum of Cd (Fig. 10(e)) shows the characteristic peaks of Cd 3d orbital by exhibiting two orbital states Cd $3d_{5/2}$ at 404.6 eV and Cd $3d_{7/2}$ at 413.0 eV. Fig. 11(a) confirms the existence of Ta peaks and all other elements (Bi, V and O) in 7% Ta-doped BV. Eventually, on analysing the core level spectrum of all elements after Ta-doping (Fig 11(b), (c), (d)) the binding energies found to be decreased. Fig. 11 (e) explicates the orbital states Ta $4d_{5/2}$ and Ta $4d_{3/2}$ of Ta 4d orbital located at 229.5 eV and 241.0 eV. Fig. 11(f) illustrates the Ta 4f orbital with Ta $4f_{7/2}$ and Ta $4f_{5/2}$ peaks at 27.3 eV and 28.3 eV along with one high O 2s peak at 25.3 eV which indicates the presence of oxygen on the atomic lattice [15-17].

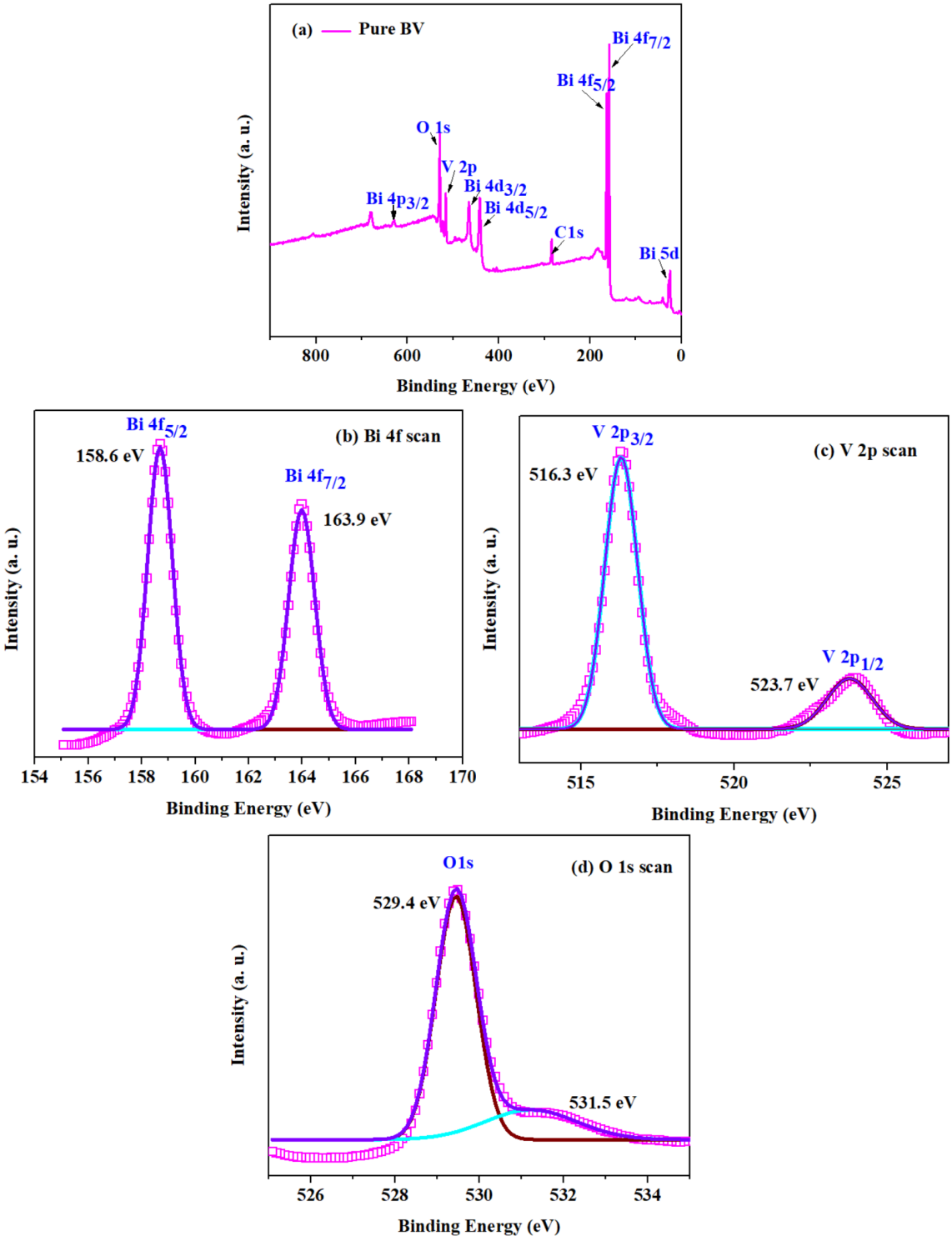

Fig. 9. (a) XPS survey spectrum of pure BV. Core level spectrum of (b) Bi 4f, (c) V 2p and (d) O 1s.

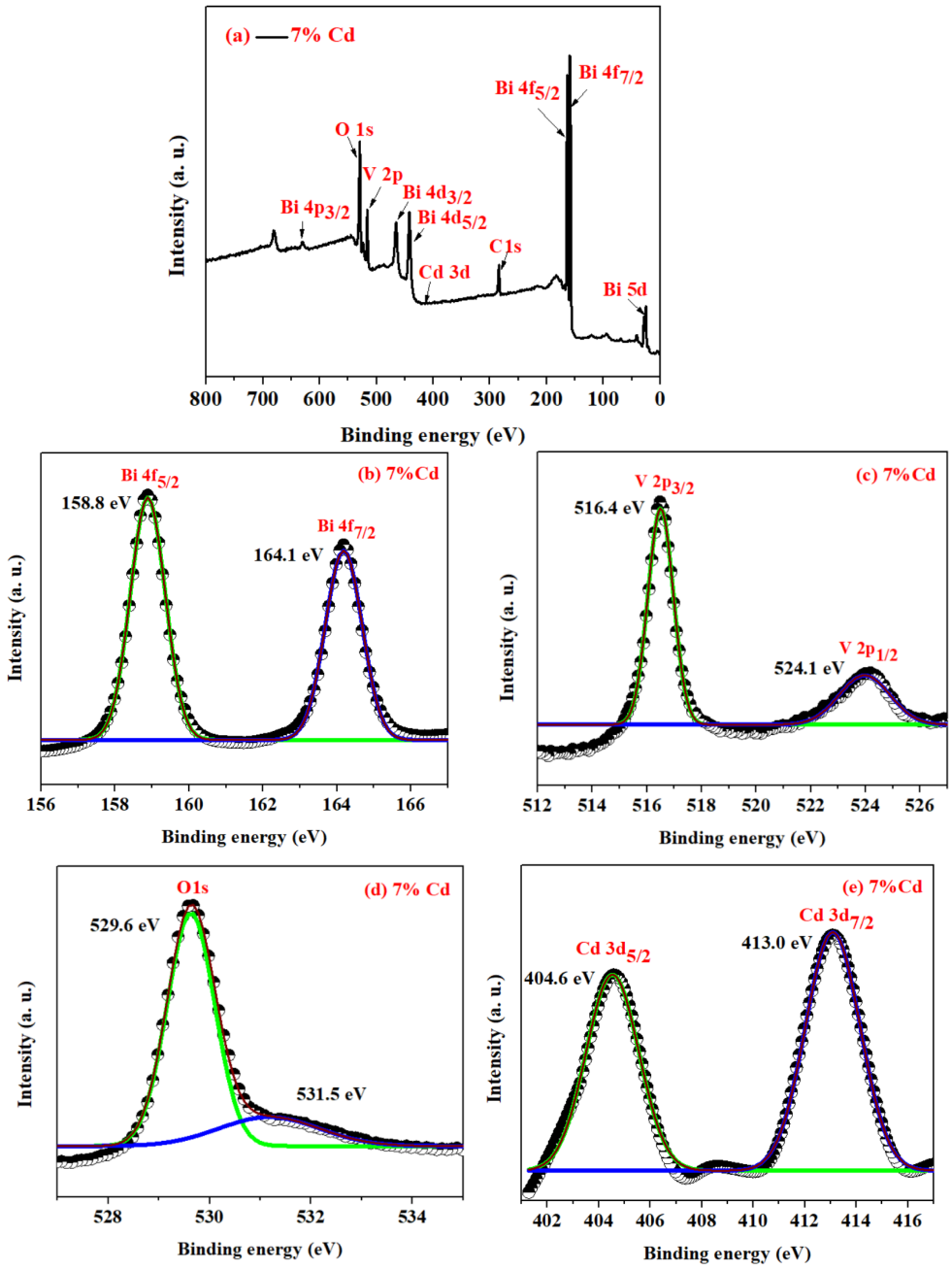

Fig. 10. (a) XPS survey spectrum of 7% Cd doped BV.

. Core level spectrum of (b) Bi 4f, (c) V 2p, (d) O 1s and (e) Cd 3d in 7% Cd-doped BV.

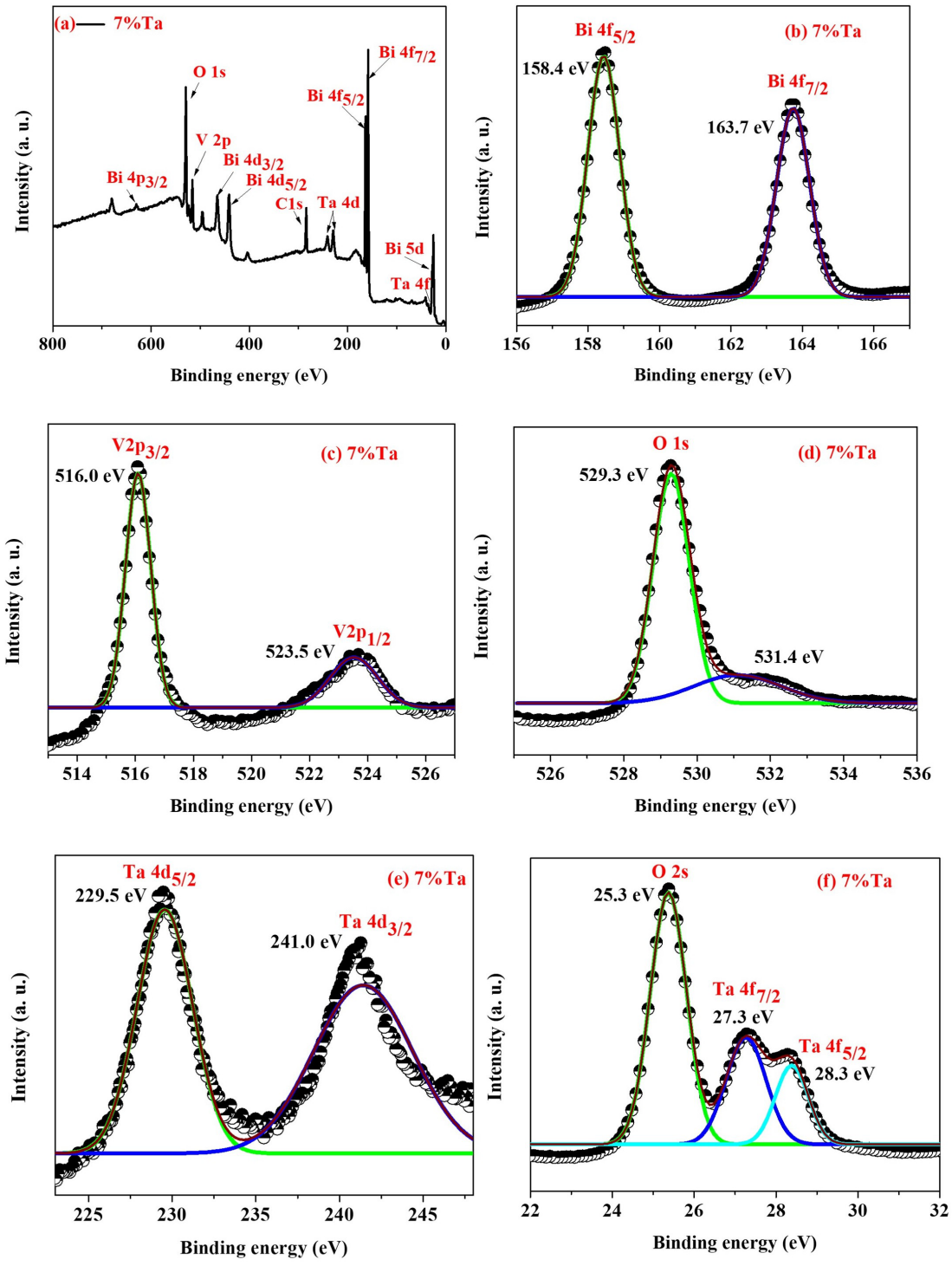

Fig. 11. (a) XPS survey spectrum of 7% Ta-doped BV. Core level spectrum of (b) Bi 4f, (c) V 2p, (d) O 1s, (e) Ta 4d and (f) Ta 4f.

3.5. Thermogravimetric analysis

TGA determines the thermal behaviour like thermal degradation, weight loss etc., of the material according to the variation in the temperature. The TGA provides the loss of weight in the sample with concern to increase of temperature. 5mg quantity of every sample was heated at a rate of 20 °C/min in the presence of nitrogen gas environment with the gas flow rate of 50 cm3/min. The weight loss of the sample was recorded from

30 °C to 600 °C. The temperature °C versus weight loss percent of all samples was plotted in the Fig 12 (a). All Cd doped samples in Fig 12 (a) except 7% Cd-doped BV showed a steady, linear, and feeble decrease in weight according to the temperature variation which proved the enormous thermodynamic stability of BV. This study confirms that BV can be operated over high temperatures without losing its stability. The weight loss of pure, 1% and 3% doped BV was merely the same. Whereas, 5% Cd-doped BV experienced relatively lesser weight loss. The plot reveals that the decrease in weight is absolutely due to the evaporation of molecules of water contained within the sample at different temperatures. Further, the curve does not account for any chemisorption and decomposition of the material. The 7% Cd-doped sample has a huge initial rise in weight due to the buoyancy effect. The buoyancy effect is attributed to the decrease or imbalance in the density of nitrogen gas that surrounds the sample, causing a modest upward force on the sample pan which is recorded by the instrument as an increase in weight of the sample. Whereas, in the case of Ta-doped samples (Fig 12 (b)) 1% doped sample initially experiences a weight gain due to the buoyancy effect but then begins to show a decreasing trend immediately after the rise [18]. All other % of Ta-doped samples had a loss in weight relative to pure BV. This denotes to us that doping Cd provides additional stability to BV as all Cd-doped samples suffer only less weight loss than pure BV and doping Ta slightly can reduce the stability of the material due to a decrease in weight compared to the pure sample which will not cause any significant change in the material's behaviour [19].

3.6. Differential scanning calorimetry

DSC is a unique tool associated with TGA for scanning the heat flow on the sample during temperature variation. It detects both the absorption and liberation of heat by the sample. It measures the heat flow in watts/gram (W/g) (Figs. 12 (c) and 12 (d)). The C_p was calculated from the data provided by DSC. Heat flow in (W/g) is multiplied by time (s) and divided by temperature (°C) to obtain C_p. C_p in (j/g °C) is plotted on y-axis and the temperature (°C) on the x-axis. The formula for specific heat capacity (C_p) is

$$C_p = \frac{Q\,t}{mT}\ \text{(j/g °C)}$$

Q is the heat flow (W), t is the time (s), m is the weight of the sample (g) and T is the change in temperature (°C) [2, 20-22]. The C_p of pure BV is very low which suit well for pyroelectric application as it can cause an increase in the values of F_I, F_V and F_D due to its inverse proportionality. All Cd-doped samples are noted to have enhanced specific heat C_p than pure BV (Fig. 12 (e)) which is appropriate for many applications viz photothermal, energy storage etc., but causes a negative effect on tunning PyFOM. Thus, the metal Cd increases the specific heat C_p which probably will decrease the PyFOM. Doping higher concentration (5% and 7%) of Ta into BV lattice leads to the reduction in C_p of pure BV (Fig. 12 (f)) thereby, creating a positive effect towards enhancing PyFOM. Thus, Ta-doped BV can suit well for pyroelectric energy harvesting purpose compared to Cd-doped BV.

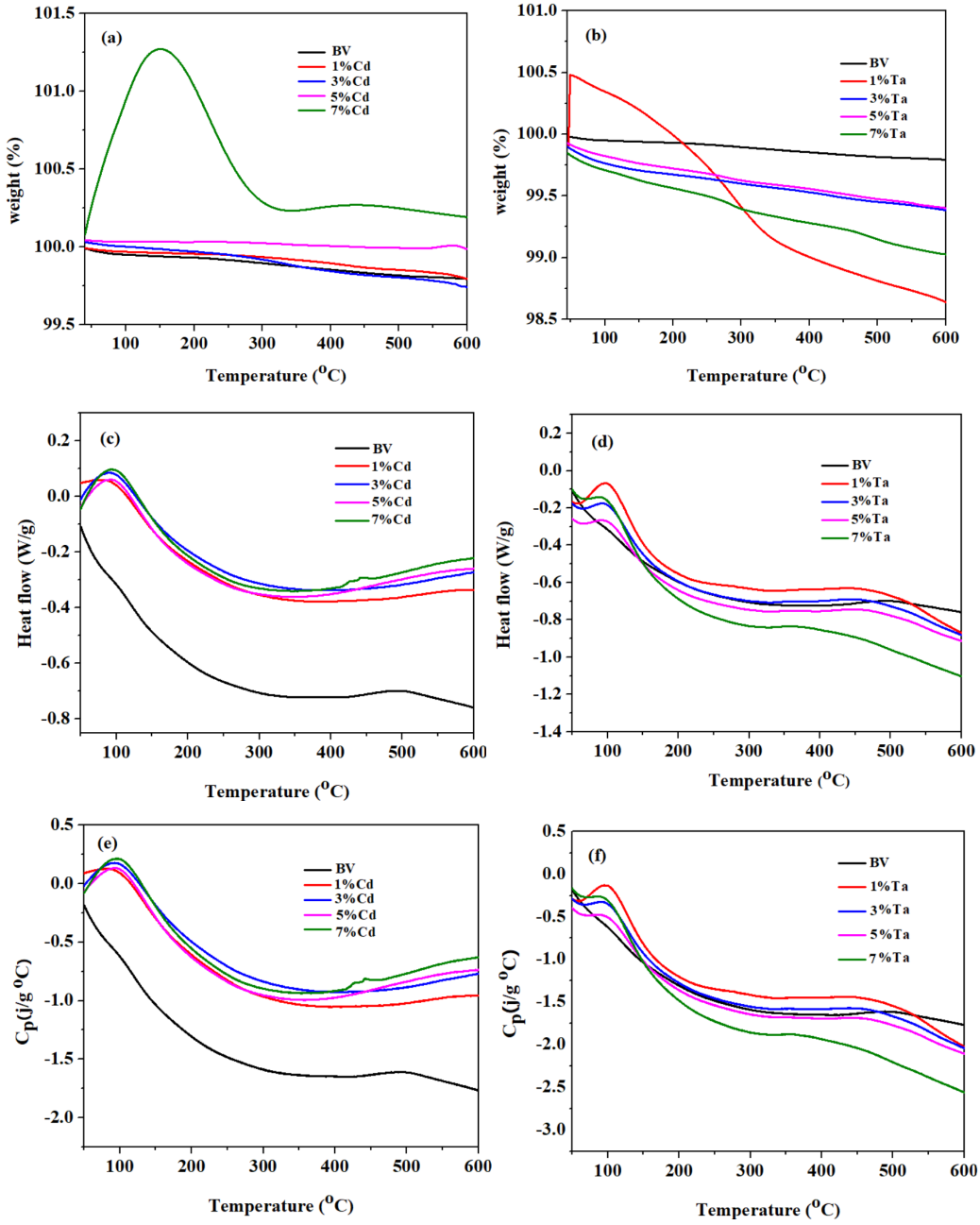

Fig. 12. Temperature versus weight (%) plot of (a) Cd and (b) Ta-doped BV. Temperature versus heat flow plot of (c) Cd and (d) Ta-doped BV. Temperature versus C_p plot of (e) Cd and (f) Ta-doped BV.

4. Conclusion

The comparative analysis of Cd and Ta-doped monoclinic scheelite BV elucidated the variation in the characteristics viz, structural, morphological, optical, elemental and thermal properties among pure, Cd and Ta-doped BV samples. All the samples were prepared by a facile hydrothermal technique. The efforts of obtaining low C_p were achieved through Ta doping which primely contributes to enhancing the PyFOM for pyroelectric energy harvesting application, on the contrary Cd doping in BV increased the C_p which can be utilized to some other applications such as photothermal, energy storage devices etc., Pyroelectric energy harvesting is planned to be done in future by extending this work.

Availability of Data and Materials

The datasets used and analyzed during the current study are available from the corresponding author on reasonable request.

Author Contributions

The author L. Balakrishnan conceived of the presented idea. The author K. Swethaa carried out the experimental work and wrote the manuscript. The authors L. Balakrishnan and M. Rajeswari supervised the work. The authors K. Swethaa and L. Balakrishnan done the samples characterization and interpretation of results. All the authors provided critical feedback and helped to shape the research, analysis and manuscript.

Acknowledgment

We would like to express our gratitude to the Department of Physics, Government College of Technology, Coimbatore, Tamil Nadu, India, for extending the experimental and characterization facilities. Thanks to all the peer reviewers for their opinions and suggestions.

Funding

This research received no external funding

Conflict of Interest

The authors declare no conflict of interest.

References

[1] E. A. Fortalnova, V. V. Murasheva, M. G. Safronenko, Bulletin of the Russian Academy of Sciences: Physics **72**, 1094 (2008); https://doi.org/10.3103/S1062873808080212.
[2] S. Patel, Journal of Materials Science: Materials in Electronics **31**, 16708 (2020); https://doi.org/10.1007/s10854-020-04226-5.
[3] M. S. Jayalakshmy, J. Philip, Sensors and Actuators A: Physical **206**, 121 (2014); https://doi.org/10.1016/j.sna.2013.12.004.
[4] S. Kausar, R. M. Munir, T. Iqbal, Journal of Inorganic and Organometallic Polymers and Materials **34**, 6071 (2024); https://doi.org/10.1007/s10904-024-03236-8.
[5] R. Prakruthi, H. N. Deepakumari, C. Mallikarjunaswamy, Journal of Materials Science: Materials in Electronics **35**, 13607 (2024); https://doi.org/10.1007/s10854-024-13609-x.
[6] D. D. Lv, J. F. Liu, Z. Zhang, Rare Metals **38**, 446 (2019); https://doi.org/10.1007/s12598-019-01210-9.
[7] W. Wei, X. Yue, H. Cui, Journal of Materials Research **28**, 3408 (2013); https://doi.org/10.1557/jmr.2013.366.
[8] T. Kansaard, M. Songpanit, R. Noonuruk, C. Wattanawikkam, W. Mekprasart, K. Boonyarattanakalin, C. K. Jayasankar, W. Pecharapa, Er-Doped, Nanomaterials **14**, 954 (2024); https://doi.org/10.3390/nano14110954.
[9] O. V. Opimakh, I. I. Kurilo, I. M. Zharskii, Inorganic Materials **50**, 415 (2014); https://doi.org/10.1134/S0020168514040141.
[10] Q. F. Lu, J. L. Li, J. Yu, L. J. Cui, B. Wang, X. J. Ma, Y. Feng, Materials Research Express **8**, 28937 (2021); https://doi.org/10.1088/2053-1591/ac3e94.
[11] S. Saranya, L. Balakrishnan, D. Sangeetha S. Lakshmi, Matéria (Rio de Janeiro) **29**, e20240427 (2024); https://doi.org/10.1590/1517-7076-RMAT-2024-0464.
[12] S. Suresh, S. Tetsuo, Inorganic Chemistry Communications **160**, 111980 (2024); https://doi.org/10.1016/j.inoche.2023.111980.

[13] A. Josephine, R. Chellathurai, R. Venkatesh, D. Arivukarasan, A. Christy, S. Monica, S. Keerthana, Materials Research Express **7**, 015036 (2020); https://doi.org/10.1088/2053-1591/ab653f.
[14] J. K. Cooper, S. Gul, F. M. Toma, C. Le, Y. S. Liu, J. Guo, J. W. Ager, J. Yano, and I. D. Sharp. The Journal of Physical Chemistry C **119**, 2969 (2015); https://doi.org/10.1021/jp512169w.
[15] M. Hellwig, A. Milanov, D. Barreca, J. L. Deborde, R. Thomas, M. Winter, U. Kunze, R. Fischer, A. Devi, Chemistry of Materials **19**, 11715 (2007); https://doi.org/10.1021/cm0630441.
[16] S. Li, Y. Cheng, Q. Wang, C. Liu, L. Xu, Design, Materials Research Express **7**, 115005 (2020); https://doi.org/10.1088/2053-1591/abc79e.
[17] Temidayo Oyetunde, Mohammad Afzaal, Mark Vincent, Ian Hillier, Paul O'Brien, Inorganic chemistry **50**, 2052 (2011); https://doi.org/10.1021/ic102309r.
[18] R. J. Demuth, A. L. D'Entremont, R. Smith, R. L. Sindelar, T. W. Knight, Nuclear Technology **210**, 2187 (2024); https://doi.org/10.1080/00295450.2024.2312019
[19] J. J. Serralta-Macías, F. Calderón-Piñar, O. García Zaldivar, D. Olguín, J. M. Yáñez-Limón. AIP Advances **11**, 065020 (2021); https://doi.org/10.1063/5.0051792.
[20] X. Feng, M. Wang, L. Li, Z. Yang, M. Cao, Z. Y. Cheng, Advanced Dielectrics **7**, 1750006 (2017); https://doi.org/10.1142/S2010135X17500060.
[21] F. Tang, S. Long, X. Yang, M. Yang, J. Quan, S. Lin, D. Ma, Y. Zhu, B. Wang, Applied Physics **51**, 395101 (2018); https://doi.org/10.1088/1361-6463/aad88d.
[22] Y. Z. Zhu, S. P. Lin, Y. Zheng, D. C. Ma, B. Wang, Journal of Materials Science **51**, 3155 (2016); https://doi.org/10.1007/s10853-015-9625-5.